Journal of Sound and Vibration 434 (2018) 442–455

Contents lists available at ScienceDirect

Journal of Sound and Vibration

journal homepage: www.elsevier.com/locate/jsvi

Modeling and experimental demonstration of heat flux driven noise cancellation on source boundary

Simon Julius, Ronald Gold, Alex Kleiman, Boris Leizeronok, Beni Cukurel*

Turbomachinery and Heat Transfer Laboratory, Faculty of Aerospace Engineering, Technion - Israel Institute of Technology, Technion City, 3200003 Haifa, Israel

ARTICLE INFO

Article history:
Received 26 July 2017
Received in revised form 5 February 2018
Accepted 6 February 2018

Handling Editor: J. Astley

Keywords:
Noise cancellation
Thermophone
Thermo-acoustic modeling
Surface heat driven acoustic emission
Noise control at source

ABSTRACT

This theoretically supplemented experimental research effort is devoted towards demonstrating the feasibility of using heat flux driven transducers, in order to annihilate undesirable acoustic fields directly at the source boundary. Using commonly available materials, a thermophone is produced and deposited on a conventional vibro-acoustic loudspeaker. Unifying the sound energy input from heat and work related processes, a holistic model is derived from first law of thermodynamics - simulating pressure fields at different locations. In the case of thermo-acoustic sound production, the formulation is complemented by an efficiency model based on Fourier heat conduction in a slab with internal unsteady generation. The ensuing sound pressure level emanating from the two sources is predicted for a broad range of measurement locations and relative excitation phase angles. The theoretical estimates are corroborated by experimental results under different conditions. For the prescribed experimental parameters, a heat-flux transducer is shown to successfully diminish the pressure wave generated by a conventional loudspeaker to ambient noise levels.

1. Introduction

Noise reduction via active sound cancellation is a trending mechanism for diminishing acoustic pollution in a multitude of sectors (aviation, energy, transportation, military etc.) [1]. The basic concept relies on local annihilation of an unwanted pressure field through the creation of an out-of-phase sound wave at the same amplitude and frequency, actively modulated by sensing elements in a control circuit. This typically involves an array of loudspeakers, which convert electric power into acoustic energy through vibro-mechanics. The geometric limitations of conventional loudspeakers prevent the effective use of these anti-phase pressure emitters from being used in a distributed manner. Therefore, the common implementation of noise cancellation is localized to the observer, rather than holistic elimination at the source.

Recently, the first theoretical studies, that predict tonal noise cancellation of a vibrational source by a heat flux emitter sharing a common emanating infinite planar boundary have been conducted [2,3]. In this model, the Navier-Stokes-Fourier equations are linearized to produce a set of unsteady one-dimensional relations of mass, momentum, and energy for calculation of density, velocity, and temperature perturbations. For far-field boundary conditions, with a sinusoidal forcing

* Corresponding author.
E-mail addresses: shimonjulius@tx.technion.ac.il (S. Julius), ronaldgo@technion.ac.il (R. Gold), alex.kleiman@technion.ac.il (A. Kleiman), borisl@technion.ac.il (B. Leizeronok), beni@cukurel.org (B. Cukurel).

https://doi.org/10.1016/j.jsv.2018.02.007
0022-460X/

Nomenclature		
a_i	[–]	Constant parameter
c_f	[m s^{-1}]	Speed of sound in a medium
c_{th}	[m s^{-1}]	Thermal speed in a medium
C_p	[J kg^{-1} K^{-1}]	Specific heat capacity at constant pressure
d	[m]	Distance between monopoles
e_f	[Jm^{-2} K^{-1} s$^{-0.5}$]	Thermal effusivity of the fluid
e_s	[J m^{-2} K^{-1} s$^{-0.5}$]	Thermal effusivity of the solid
f	[Hz]	Input frequency
g	[W m^{-3}]	Internal generation
h	[W m^{-2} K^{-1}]	Heat transfer coefficient
Kn	[–]	Knudsen number
L	[m]	Thermophone thickness
p	[Pa]	Pressure
$\overline{P}_{in}$	[W]	Input power
r	[m]	Pressure wave radius
r_0	[m]	Pressure wave radius for a single forcing period
r_k	[m]	Distance from the kth point source
R_g	[J kg^{-1} K^{-1}]	Gas constant
S	[m^2]	Total sound source area
T	[K]	Temperature
V_f	[m^3]	Volume of the sound wave

distribution for both the vibrating boundary and the oscillating heat flux, the optimal sound reduction is obtained when the sound amplitude and the frequencies of the two signals are identical, however out of phase. In addition, the ratio between thermal and kinetic energies is suggested to depend on the particular wavelength and fluid properties.

Although only described theoretically in the absence of practical considerations, the concept of heat flux driven active noise cancellation can be considered a disruptive technology. With a static and surface-distributed sound emitter, the undesirable acoustic fields can be annihilated directly at the source boundaries, holding promise for truly silent bodies. Building upon the existing knowledge in analytical predictions on the interaction of surface heat with sound emanating from a boundary, and heat driven acoustic field generation in solid media, this effort is devoted to modeling and experimental demonstration of using a static secondary heat-flux driven transducer to achieve noise cancellation from a vibrating source. Thereby, the work is intended to bridge the gap in scientific and engineering knowledge towards feasible thermoacoustic noise cancelation in solid-gas interfaces.

In order to achieve this goal, one of the critical considerations involves the mechanism of periodic heat generation at the boundary. Pressure field stimulation and sound production via Joule heating has been studied since the late 19th century [4]. The term "thermophone" is coined two decades later [5], to define an acoustic transmitter capable of producing sound through high frequency thermal oscillations. Thermophones behave as electrical resistors, where an alternating electrical current is converted to produce surface heat flux fluctuations and, consequently, pressure waves in the surrounding fluid, absent of mechanical motion [6]. However, there is no clear consensus in the literature as to the correct approach to modelling thermophone sound production [7–14]. At the turn of the 21st century, the thermophones regained the interest of the scientific community and advanced designs (such as suspended arrays of aluminum wires, carbon nanotubes, and graphene) are developed to explore the efficiency and performance envelopes of heat flux sound sources [9,15–23]. Moreover, significant efforts have been invested to characterize the impact of the deposition substrate [10,14], and thermophone behavior in different gaseous and liquid media [8,24–26].

Along these lines, a thermophone is produced using commonly available materials and deposited on a conventional vibro-acoustic speaker, simulating the unwanted noise source. Both the thermal transducer and the loudspeaker are experimentally characterized by microphone measurements for various amplitudes and frequencies. The empirical results are correlated with analytical thermo-acoustic conversion and 3-D sound propagation models in a novel theoretical framework, yielding the efficiency of the thermophone. With the appropriate knowledge of the system characteristics, at an exemplary frequency, the constructive and destructive interference of the two emitters are presented for varying phase differences in different measurement locations. According to the authors' knowledge, this is the first practical demonstration of the heat flux driven noise cancellation in scientific literature.

2. Experimental setup

A dedicated experimental facility, the layout of which is depicted in Fig. 1, is used to study the interaction between vibro- and thermo-acoustic sources. The experiments are conducted in a soundproof box with dimensions of $0.5 \times 0.5 \times 1.0$ m^3. The test chamber is acoustically insulated with acoustic foam to minimize scatter and promote the dampening of wall reflections. While the box is shut, an IR camera is employed to monitor the experimental set-up.

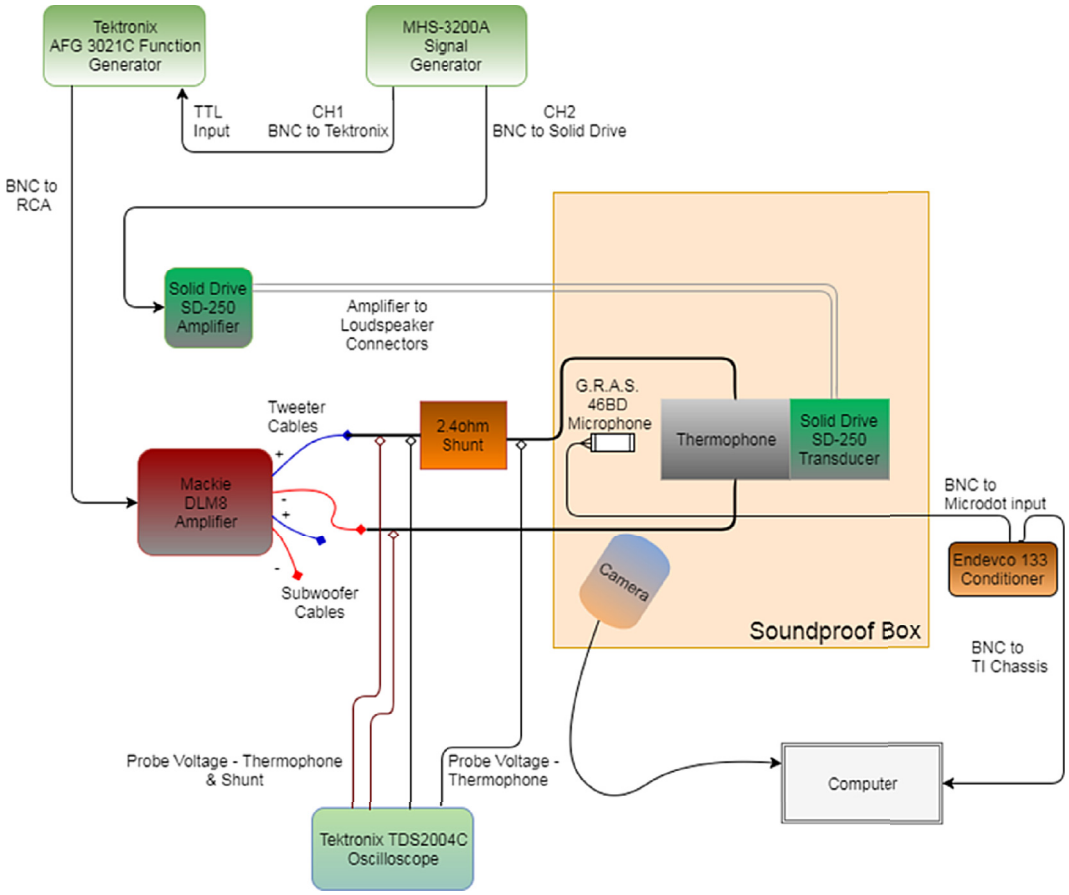

Fig. 1. Experimental set-up schematic.

The existing thermo-acoustic literature concurs that the transducer heat capacity per unit volume must be low [7,15]. This is typically achieved by using ultrathin sheets such as graphene, or carbon nanotube wires [15,27]. However, growing carbon nanotubes on solid backing can drastically modify their properties, and the process of material selection is further complicated by their complex interactions [28]. Therefore, in order to demonstrate the feasibility of noise cancellation by a heat flux source, a more pragmatic manufacturing method is used. Aremco Pyro-Duct 597 silver paste and aluminum nitride substrate are chosen due to their chemical stability (up to $\sim 900\,^{\circ}\mathrm{C}$ and $\sim 1400\,^{\circ}\mathrm{C}$ respectively), and relatively high thermal conductivity ($9\,\mathrm{W\,m^{-1}K^{-1}}$ and $180\,\mathrm{W\,m^{-1}\,K^{-1}}$ respectively). To create the surface, 1.1 g of silver paste are first dissolved in 100 ml of cold water, and 10 ml of the resultant solution are drop-cast onto the aluminum nitride substrate with dimensions of $5 \times 5 \times 0.07$ cm.. The coated aluminum nitride is then cured for 25 min at $100\,^{\circ}\mathrm{C}$ to form a 20 μm uniform film, the thickness of which is measured by Fischer FMP20 Dualscope. Although this coating thickness can be minimized in order to increase the efficiency of heat-to-sound conversion, the relatively thick transducer is used in order to ensure surface uniformity and homogeneity at this stage of investigation. Two edges of the plate are coated with aluminum tape and covered with conductive silver ink from MG Chemicals. These terminals are further sealed with a copper adhesive coating, on which thin wires are soldered to create connection terminals.

A Mackie DLM8 co-axial loudspeaker amplifier, capable of applying frequencies ranging from 75 Hz to 20 kHz, is used to power the thermophone transducer. Frequencies below 2 kHz are delivered through the DLM8 sub-woofer, while the rest are taken from the DLM8 tweeter. In order to match the required load impedance of the amplifier, a bank of five parallel 10 Ω resistors (each rated to 100 W) is attached in series to the thermal speaker. The power input to the thermo-acoustic speaker module is evaluated by measuring the potential difference across the resistor bank and across the entire circuit using Tektronix TDS2004C oscilloscope, Fig. 1. The final thermophone transducer has a nominal total resistance of 0.7 Ω, and is attached to a 5 mm thick aluminum base plate using double-sided Davik DS4341 thermally resistant tape, Fig. 2.

Elevating the subassembly on four rubber-damped 10 cm bolts, a vibro-acoustic Solid Drive SD-250 transducer is screwed onto the base underside directly below the thermophone plate, Fig. 3. During its operation, the Solid Drive applies vibrations to the aluminum base, transforming the entire surface into a rigid diaphragm. The system's structural behavior is characterized in COMSOL Multiphysics simulation using an isotropic linear elastic model with constrained bolt locations. Static 1 Pa

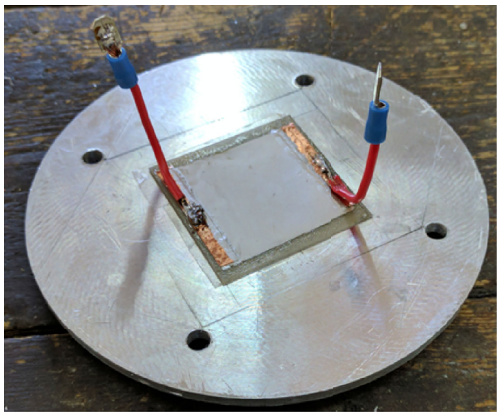

Fig. 2. Thermophone transducer.

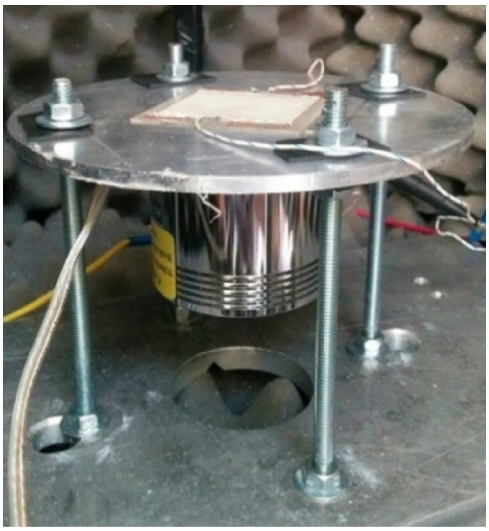

Fig. 3. Thermophone, aluminum base plate and Solid Drive set-up.

load is imposed on the boundary where the loudspeaker resides. The ensuing displacement is presented in Fig. 4, where the maximum value is observed towards the center of the plate with high degree of angular uniformity and a platykurtic distribution. Towards the edges, large spread in the plate displacement can be observed due to the nature of the individually bolted boundaries.

This mechanical transducer is powered through the Solid Drive amplifier circuit, which receives a signal from a MHS-3200A signal generator. In order to synchronize the two sound sources, another channel of the signal generator delivers a TTL signal, which drives a Tektronix AFG3021C function generator connected to the thermophone amplifier, Fig. 1. Once triggered, the function generator outputs a signal at half the frequency provided to the mechanical speaker at a pre-set phase angle. This frequency reduction is necessary as the power delivered into the thermophone results in a double heating cycle per period, whereas the mechanical speaker experiences a single mechanical work cycle during same time. As a result, both the mechanical and thermophone transducers are tuned to produce acoustic excitations at the same tone.

The sound pressure level and frequency content is quantified via a G.R.A.S. 46BD condenser microphone placed above the aluminum base plate, in the geometric center of the plane. The relative height of the microphone can be varied by a linear positioner. Locations are selected to be in the far field, while additional efforts were made to minimize the surrounding interferences and resonance effects towards achieving maximal signal to noise ratio. The resulting signal is amplified with an Endevco 133 conditioner and recorded via National Instruments DAQ9205 data acquisition module. The sound pressure amplitude is calculated using a Fast Fourier Transform, with a Flat-Top windowing scheme, which maintains high accuracy in the peak response magnitude (typical FFT peaks are very sharp with no evidence of harmonics).

The final experimental procedure consists of the following three steps: The vibro-acoustic source is switched on and tuned to a specific frequency and amplitude. Switching off this mechanical transducer, the heat-flux source is turned on with halved

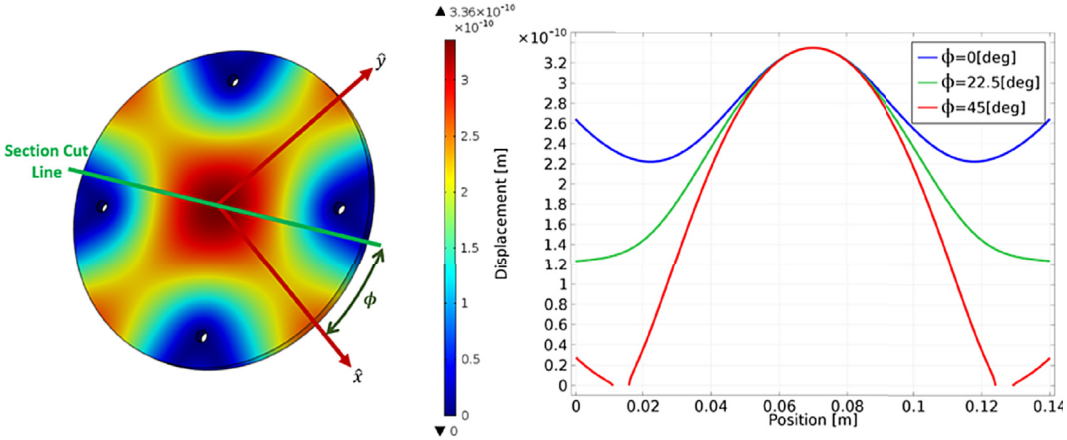

Fig. 4. Structural displacement of the aluminum base due to Solid Drive mechanical oscillations (left) and base plate displacement profiles at various x-y plane section cuts (right).

frequency input and brought to the same sound pressure level for the identical reference measurement location. Both vibro-acoustic and thermo-acoustic transducers are then powered and allowed to reach a steady periodic state of operation. While maintaining all the other parameters, the relative phase of the excitations is altered. The empirical data collected is initially used to characterize the acoustic performance of the thermal and the mechanical transducers via semi-analytical models.

3. Thermodynamic model

In thermophone devices, the impact of pressure waves on the heat flux transduction process has been demonstrated to be negligible [29], and therefore the sound creation and propagation can be considered independent of the heat generation. An intuitive understanding of the phenomenon is garnered by studying the sound production mechanism as a quasi-static process [14]. As the Navier-Stokes-Fourier model described in Refs. [2,3] inherently assumes an infinite source boundary, it is unsuitable in practice. Therefore, this weighted point source approach fits better in the current framework.

Independent of the sound generation mechanisms involved, the thermal wave emanating from a surface can be modeled as a closed thermodynamic system, whose volume (V_f) is a function of the sound wave propagation radius for a single period. Assuming a homogeneous acoustic medium with a uniform flat boundary, the mean pressure wave radius (r_0) for a single forcing period is described as [26]

$$r_0 = \frac{\pi c_{th}}{\omega}, \tag{1}$$

where the thermal velocity $c_{th} = \sqrt{2/\gamma}\, c_f$, c_f is the speed of sound in the medium and ω is the angular frequency. Hence, V_f is the hemispherical volume covered by a single cycle pressure wave, spanning a radius of r_0 from the source:

$$V_f = \frac{4\pi^4}{3}\left(\frac{\sqrt{2/\gamma}\, c_f}{\omega}\right)^3. \tag{2}$$

For a general quasi-static closed system, the first law of thermodynamics in Fourier space states that

$$\Delta\overline{U} = \Delta\overline{Q} + \Delta\overline{W}, \tag{3}$$

where $\Delta\overline{Q}$ is the net quantity of heat supplied to the system, $\Delta\overline{U}$ is the change in the mean internal energy of the system and $\Delta\overline{W}$ is the net work done on system [30].

The vibrations of a typical loudspeaker adiabatically generate sound pressure by only applying mechanical work onto the small fluid volume V_f surrounding the transducer:

$$\Delta\overline{W} = \Delta\overline{U} = \Delta\left(\overline{p}V_f\right) = V_f\Delta\overline{p}_v, \tag{4}$$

where $\Delta\overline{p}_v$ is the pressure due to the vibroacoustic effect. In contrast, as the thermophone is a mechanically static sound emitter [6], the genesis of a pressure wave is exclusively associated with the heat input ($\Delta Q = mC_p\Delta T$) [30]. Assuming ideal gas law,

$$\Delta\overline{Q} = \Delta\overline{U} = \Delta\left(\overline{\rho}V_f C_p\overline{T}\right) = V_f C_p \Delta\left(\overline{\rho}_{hf}\overline{T}_{hf}\right) = \frac{V_f C_p}{R_g}\Delta\overline{p}_{hf}, \tag{5}$$

where $\Delta\overline{p}_{hf}$ is the pressure due to the heat flux, ρ is the density, T is the temperature and C_p is the specific heat capacity at constant pressure. In order to have no change in internal energy, the sound created by the vibrating source must be negated by an equal magnitude and opposite phase pressure wave of the thermophone. Accordingly, the cancellation between the two sources will happen at a work to heat energy ratio of $\frac{R_g}{Cp} = \frac{\gamma-1}{\gamma}$, where R_g is the gas constant and γ is the ratio of specific heats. Although derived from a different set of physical equations, the observation is identical to that predicted in the low frequency limit from the linearized Navier-Stokes-Fourier equations [2].

Then, irrespective of the energy source for sound creation, a generalized expression can be written as

$$\Delta\overline{U} = V_f a_i \Delta\overline{p}_i, \tag{6}$$

where a_i is a constant parameter that corresponds to $a_{hf} = \frac{C_p}{R_g} = \frac{\gamma}{\gamma-1}$ and $a_v = 1$. Accordingly, the power input, P_{in}, of the thermal source during one period $(2\pi/\omega)$ is

$$\overline{P}_{in} = \frac{1}{\eta(\omega)} V_f \frac{\omega}{2\pi} a_i \Delta\overline{p}_i \tag{7}$$

where η is the sound production efficiency, defined by the proportion of the Joule heating that contributes to the oscillating component of the surface heat flux. Therefore, combining with Eq. (2), the pressure over one period is

$$\Delta\overline{p}_i = \frac{3\eta(\omega)\overline{P}_{in}\omega^2}{2\pi^3 a_i \left({}^{2}/_{\gamma}\right)^{3/2} c_f^3}, \tag{8}$$

4. Sound propagation

Neglecting sound attenuation, a pressure wave propagates from the surface while obeying the following relationship [26]:

$$\Delta\overline{p}_i(r) = \Delta\overline{p}_i(r_0)\frac{r_0}{r}, \tag{9}$$

where r is the pressure wave radius. Combining Eq. (1) and Eq. (8) into Eq. (9), a single source point expression can be obtained as

$$\Delta\overline{p}_i(r) = \frac{3\omega\gamma\eta(\omega)\overline{P}_{in}}{4\pi^2 r a_i c_f^2}. \tag{10}$$

Taking into account phase and attenuation via the Kirchhoff-Helmholtz integral [26], the pressure from a monopole source is characterized by:

$$\Delta\overline{p}_i(r) = \frac{3}{\pi}\cdot\frac{\omega}{4\pi r}\cdot\overline{P}_{in}\eta(\omega)\cdot\frac{\gamma}{a_i c_f^2}\cdot e^{-\frac{\omega^2 r}{2\rho c_f^3}\left(\frac{4}{3}\mu_d+\mu_v+\kappa\left(\frac{\gamma-1}{C_p}\right)\right)}\cdot\left|e^{i\left(\frac{\omega r}{c_f}\right)}\right|, \tag{11}$$

where, μ_d and μ_v are the dynamic and volumetric fluid viscosities respectively, C_p is the heat capacity, κ is the thermal conductivity and γ is the ratio of specific heats.

Illustrating the effect of attenuation at standard atmospheric conditions, Fig. 5 presents the sound pressure in air at a distance of 1 m from a constant power source for different excitation frequencies. It is evident that the attenuation effect cannot be neglected for excitation frequencies above 30 kHz.

Extending the formulation in Eq. (11) to planar sources, the emitting surface is modeled by a series of n monopoles with sufficient density. To accurately capture the wave interferences, the distance d between the monopoles should be [31]

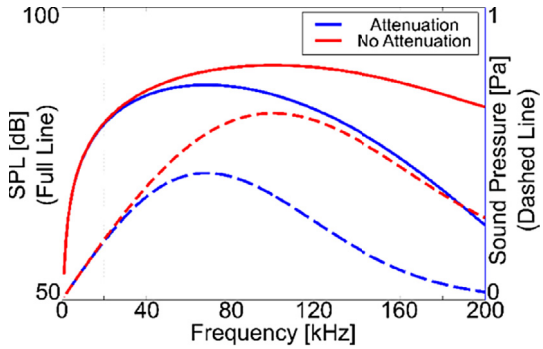

Fig. 5. Effect of frequency on sound attenuation in terms of SPL and sound pressure for air at standard atmospheric conditions.

$$d_i \leq \frac{2\pi c_f}{5\omega}. \tag{12}$$

Assuming a square source geometry, the number of necessary points is

$$n \geq \frac{S_i}{d_i^2} \geq \frac{25\omega^2 S_i}{4\pi^2 c_f^2}, \tag{13}$$

where S_i is the total area of the sound source. The magnitude, phase difference, and ensuing interference between the pressure waves emanating from individual point sources is accounted for by performing a summation of their individual contributions at the interrogation point

$$\Delta\overline{p}_i(r) = \sum_{k=1}^{k=n} \Delta\overline{p}_i(r_k), \tag{14}$$

where the interrogation point r_k is defined in 3D Cartesian space for the kth radiating point source as

$$r_k = \left((x - x_k)^2 + (y - y_k)^2 + (z - z_k)^2\right)^{\frac{1}{2}}. \tag{15}$$

Combining together the energy balance and sound propagation models, the final expression for pressure wave propagation from a square emitting surface divided into n point sources is

$$\Delta\overline{p}_i(r) = \sum_{k=1}^{k=n} \frac{3}{\pi} \frac{\omega\gamma\eta(\omega)\overline{P}_{in}}{4\pi r_k a_i c_f^2} e^{-\frac{\omega^2 r_k}{2\bar{\rho}c_f^3}\left(\frac{4}{3}\mu_d + \mu_v + \kappa\left(\frac{\gamma-1}{C_p}\right)\right)} \cdot \left| e^{i\left(\frac{\omega r_k}{c_f} + \phi\right)} \right|, \tag{16}$$

where ϕ is a pre-set phase lag term. In practice, it is conceivable that the thermo- and vibro-acoustic emission surfaces may not be identical in size and shape, thus requiring a non-trivial phase difference for sound cancellation.

Accordingly, the ensuing pressure field resulting from the heat flux and vibro-acoustic excitations is the spatial superposition of the two independent waves emanating from the two sources:

$$\Delta\overline{p}_{tot}(r, \phi) = \Delta\overline{p}_{hf}(r) + \Delta\overline{p}_v(r, \phi). \tag{17}$$

5. Acoustic characterization of heat flux excitation source

In order to quantify the pressure field of the heat flux source, microphone measurements are conducted at a distance of 3.5 cm from the transducer. Powering only the thermophone at constant 25 W, the sound pressure level variation with frequency is recorded, depicted in Fig. 6. The maximal sound pressure of $\sim$ 70 dB is obtained at a frequency of $\sim$ 7.5 kHz. No sharp peaks are observed in the range of $0.1 - 40$ kHz, suggesting that the source exhibits no resonances in the experimental range. However, there is evidence of frequency dependent weak interferences as a result of reflections within the soundproof box.

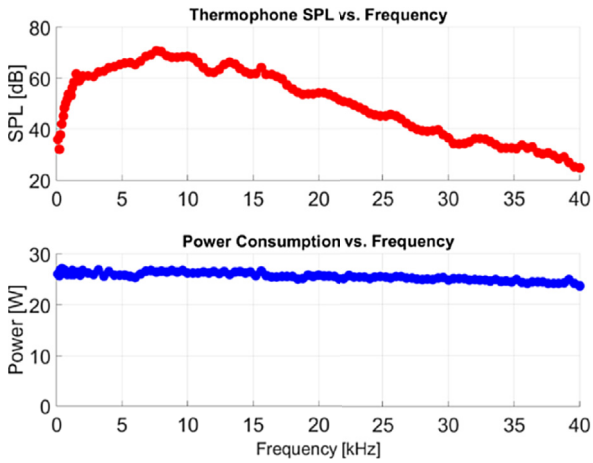

Fig. 6. Thermophone sound pressure as a function of frequency at constant input power of 25 W at a 3.5 cm height from the aluminum base (in the far field up to 25 kHz).

The efficacy of the thermal source is investigated by producing sound at different frequencies, while maintaining constant SPL of $\sim$ 50 dB, Fig. 7. The study is conducted by ramping the input power up from initial 5 W and determining the minimum power required for maintaining constant 50 dB SPL at each frequency. Outside the range of $3-15$ kHz, a higher power is required for the same SPL. Hence, the investigated frequency range is limited to values less than 25 kHz. Above the limit, the input power required to maintain 50 dB rises beyond 60 W. As this corresponds to heat generation greater than 24 kW m^{-2}, excessive power input across the device may cause permanent damage. However, it is unclear whether this increased power demand is also associated with deteriorating sound propagation or with the inefficiency of the transducer. This phenomenon cannot be justified by thermal saturation alone [32], as it would display a decrease in power requirement trend whereas the experiment shows otherwise. In order to resolve this ambiguity, the thermophone efficiency $\eta(\omega)$ needs to be evaluated.

6. Thermophone efficiency $\eta(\omega)$

There is a plethora of available literature relating to the thermophone performance modeling of ultrathin structures with low heat capacity per unit volume [9,11,13,14,22,23,33]. However, due to the selected material and geometry of the device used in this paper, the available performance models are ill-suited. For example, if the transducer thickness tends to zero, it has been shown that the heat flux amplitude is independent of frequency [33]. In contrast, for finite thickness bodies, this assumption cannot be relied upon.

In this light, a simple classical Fourier heat conduction model of a 1D slab with generalized non-homogenous Robin boundary conditions is used to capture the frequency dependent efficiency trends to a high degree of fidelity. Described in Fig. 8, this thermal model can be solved analytically [34].

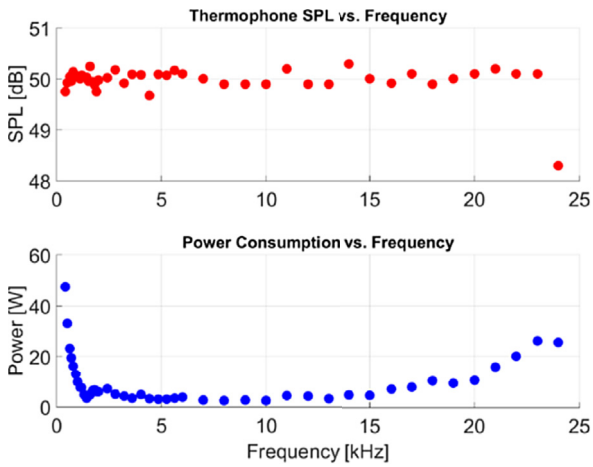

Fig. 7. Thermophone input power as a function of frequency at constant 50 dB SPL at a 3.5 cm height from the aluminum base (in the far field).

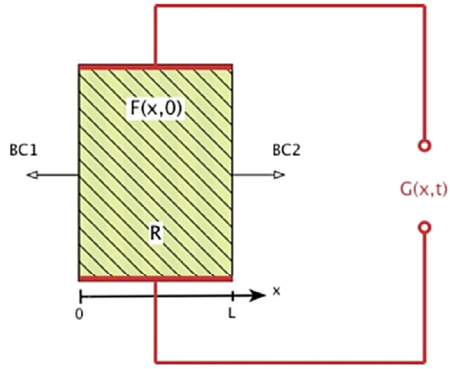

Fig. 8. Thermophone thermal model.

The governing equation is

$$\frac{1}{\alpha}\frac{\partial T}{\partial t}=\frac{\partial^2 T}{\partial x^2}+\frac{1}{\kappa}g(x,t), \tag{18}$$

with generalized non-homogeneous boundary conditions

$$\pm\kappa\frac{\partial T(x,t)}{\partial x}\bigg]_{\substack{x=0\\x=L}}+h_{1,2}T(x,t)\big]_{\substack{x=0\\x=L}}=f_{1,2}(t). \tag{19}$$

This partial differential equation can be readily solved by applying the separation of variables and integral transform techniques in the spatial dimension. The general solution is found to be:

$$T(x,t)=\sum_{m=1}^{\infty}\mathrm{e}^{-\alpha\beta_m^2 t}\cdot K(\beta_m,x)\cdot\left[\overline{F}(\beta_m)+\int_{t'=0}^{t}\mathrm{e}^{\alpha\beta_m^2 t'}\cdot A(\beta_m,t')\cdot dt'\right], \tag{20}$$

where,

$$\begin{aligned}
A(\beta_m,t)&=\tfrac{\alpha}{\kappa}\overline{g}(\beta_m,t)+\alpha\left[\frac{K(\beta_m,x)}{\kappa}\bigg|_{x=0}\cdot f_1(t)+\frac{K(\beta_m,x)}{\kappa}\bigg|_{x=L}\cdot f_2(t)\right],\\
\overline{g}(\beta_m,t')&=\int_0^L K(\beta_m,x')\cdot g(x',t')\cdot dx',\\
\overline{F}(\beta_m)&=\int_0^L F(x')\cdot K(\beta_m,x')\cdot dx',
\end{aligned}$$

$$K(\beta_m,x)=\frac{\left(\frac{h_1}{\kappa}\right)\cdot\sin(\beta_m x)+\beta_m\cos(\beta_m x)}{\left[\left(\beta_m^2+\left(\frac{h_1}{\kappa}\right)^2\right)\cdot\left(\frac{\left(\frac{h_2}{\kappa}\right)}{\beta_m^2+\left(\frac{h_2}{\kappa}\right)^2}+L\right)+\left(\frac{h_1}{\kappa}\right)\right]^{\frac{1}{2}}}. \tag{21}$$

β_m are the roots of the transcendental equation

$$\tan(\beta_m L)=\frac{\left(\frac{h_1}{\kappa}\beta_m+\frac{h_2}{\kappa}\beta_m\right)}{\left(\beta_m^2-\frac{h_2 h_1}{\kappa^2}\right)}. \tag{22}$$

In the scope of this work, the transducer thickness and area are $L=2\cdot10^{-5}$ m and $S_{hf}=0.05\times0.05$ m^2 respectively. From the specifications sheet of Aremco Pyro-Duct 597, thermal conductivity is $\kappa=9.1$ W m^{-1}K^{-1}. Moreover, the density and specific heat capacity is estimated as $\rho=1470$ kg m^{-3} and $C_p=708$ J kg^{-1}K^{-1} respectively. The initial transducer temperature is uniformly ambient, $F(x)=0$. The heat is generated internally by the Joule effect, $g(t)=\left(P_{in}\sin^2\left(\frac{\omega t}{2}\right)\right)\Big/S_{hf}L$, and

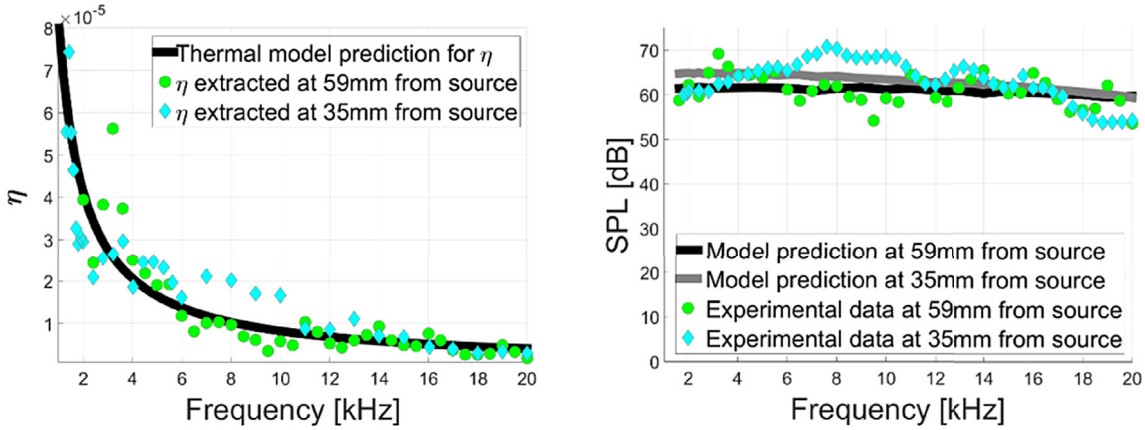

Fig. 9. Comparison of thermophone model with experimental results as a function of frequency in terms of efficiency $\eta(\omega)$ (left) and reconstructed sound pressure level (right) in the far field.

distributed according to thermal product ratio $\frac{e_f}{e_s+e_f}$. In this configuration, 99.97% of the generated heat is estimated to dissipate through the base side of the transducer. Thereby, the boundary condition of the aluminum plate side is $h_2 = 0$, and $f_2(t) = 0.9997P_{in}/S_{hf}$. The heat is transferred on the air side by natural convection, where $h_1 = 9\ W\ \mathrm{m}^{-2}\mathrm{K}^{-1}$ and $f_1(t) = 0$.

According to this thermal model, the thermal efficiency of the thermophone transducer is calculated from

$$\eta(\omega) = \left\{ \frac{\kappa \cdot \left[\frac{\partial T}{\partial x}\Big|_{max} - \frac{\partial \overline{T}}{\partial x} \right]_{x=0}}{\left(\frac{P_{in}|_{max}}{S_{hf}} \right)} \right\}. \tag{23}$$

Alternatively, the efficiency is given as follows in Fourier space:

$$\eta(\omega) = \left\{ \frac{\kappa \cdot \frac{\mathrm{d}\overline{T}}{\mathrm{d}x}\Big|_{\substack{x=0 \\ f=\omega/2\pi}}}{\left(\frac{\overline{P}_{in}}{S_{hf}} \right)} \right\}. \tag{24}$$

This frequency dependent efficiency distribution is presented in Fig. 9a by the black line. In order to validate the analytical model, experimental data is acquired for constant 25 W power in the $1.5 - 20$ kHz frequency range at a distance of 5.9 cm and 3.5 cm. The obtained sound pressure level is charted in Fig. 9b with green and blue scattered points respectively. Using these measurements, heat flux efficiency $\eta(\omega)$ is calculated by solving the acoustic model in Eq. (16). In this case, the equation is solved iteratively, with a convergence criterion of $\mathscr{O}(10^{-3}\ \mathrm{dB})$.

The ensuing spread of experimentally estimated efficiencies are represented by the scatter points on Fig. 9a. Similarly, using Eq. (16), the theoretical efficiency model can also be translated to a predicted sound pressure level at the experimental conditions, black and grey lines in Fig. 9b. Overall, the thermal model shows good agreement with the experimental results, suggesting that classical Fourier heat conduction processes alone can successfully capture the sound production behavior for this particular thermophone device. Relating back to the thermophone power consumption measurements for a constant SPL (Fig. 7), the increase in power demand at higher frequencies is therefore shown to stem from the overall reduction in device efficiency.

7. Noise cancellation by a secondary heat-flux source

Having fully characterized the thermophone speaker, the investigation attempts at using the linear superposition to achieve noise cancellation from a vibro-mechanical noise source. The baseline SPL response of the Solid Drive speaker is characterized at 3.5 cm for constant input signal amplitude across a frequency range, Fig. 10. The pressure level varies by several orders of magnitude around certain frequencies, namely 1.1 kHz, 2 kHz, 5.6 kHz, 10 kHz, 15.6 kHz and 21.2 kHz. It is conceivable that this is associated with mechanical resonance behavior observed in most loudspeakers. In order to confirm this hypothesis, an eigenmode analysis is conducted on the Aluminum plate using COMSOL Multiphysics, where the

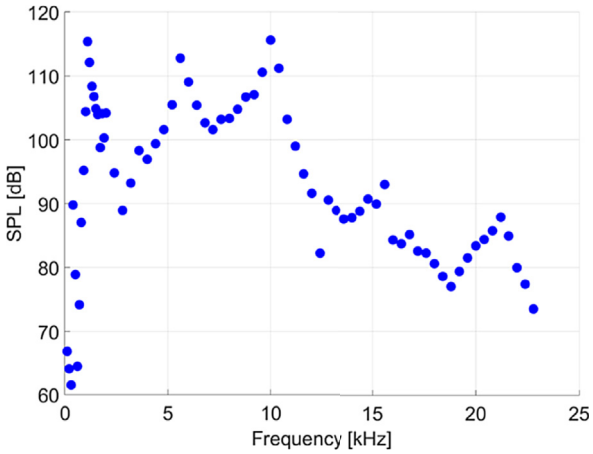

Fig. 10. Solid Drive sound pressure as a function of frequency in the far field at constant input signal amplitude at a 3.5 cm height from the aluminum base.

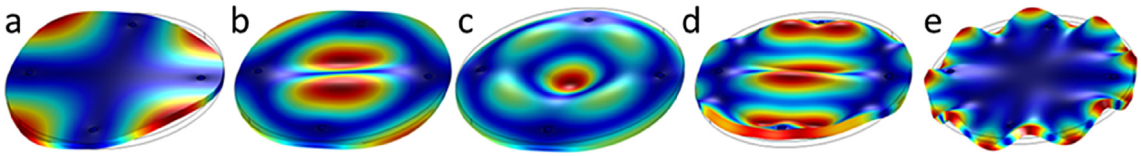

Fig. 11. Base plate eigenmodes corresponding to resonance peaks of (a) 2000 Hz, (b) 5600 Hz, (c) 10000 Hz, (d) 15600 Hz, (e) 21200 Hz.

slab is constrained at the bolt locations. The resulting eigenmodes of the simulation are depicted in Fig. 11, the frequencies of which correlate closely with the experimental findings.

The constructive/destructive interference of the heat-flux and the mechanical sources is studied at an exemplary 8 kHz frequency, away from the mechanical resonances. The vibro-acoustic source is excited to achieve 68 dB at a distance of 1.42 cm. In order to create an equal magnitude pressure wave by a heat flux source, the required thermophone input power can be calculated using the acoustic propagation and sound generation efficiency models, Eq. (16) and Eq. (24) respectively. For this particular case, the power input to the heat flux transducer is estimated to be 27.8 W. In order to confirm that the resulting pressure amplitude is equal for both the thermophone and the Solid Drive, each transducer is excited in the absence of the other sources. This is depicted by the overlaying blue and dashed red lines in Fig. 12. Then, according to Eq. (17), the effect of combining these pressure sources can be predicted at different relative phase angles by individually modeled vibro- and thermo-acoustic transducers, Eq. (16). The ensuing sound pressure level is predicted by the yellow curve in Fig. 12, suggesting varying extent of interference for different phase angles and complete local noise cancellation at 225°, where the measurements indicate 25 dB (within the background noise). For two 1-D transducers, the destructive interference would have occurred at 180°. However, given that the two source areas are of different shape and size, the shift is expected. In following, the predictions are confirmed experimentally by varying the relative phase of the signal input to the vibro-

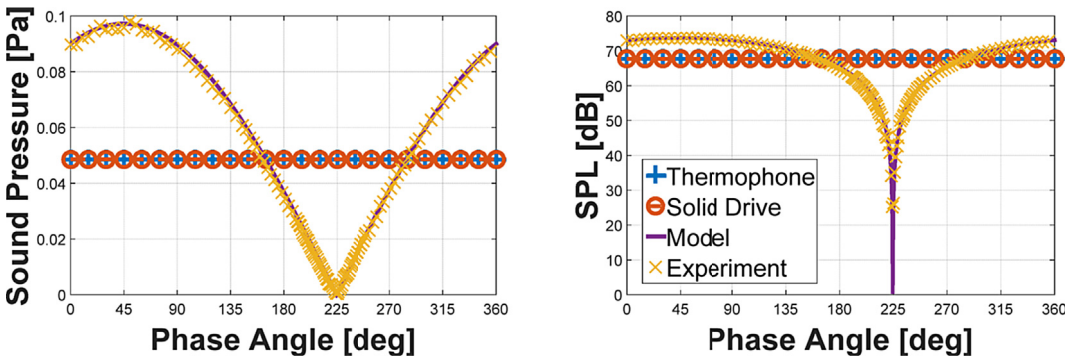

Fig. 12. Combined sound pressure (left) and SPL (right) of thermophone and Solid Drive as a function of relative phase at a constant frequency of 8 kHz (in the far field).

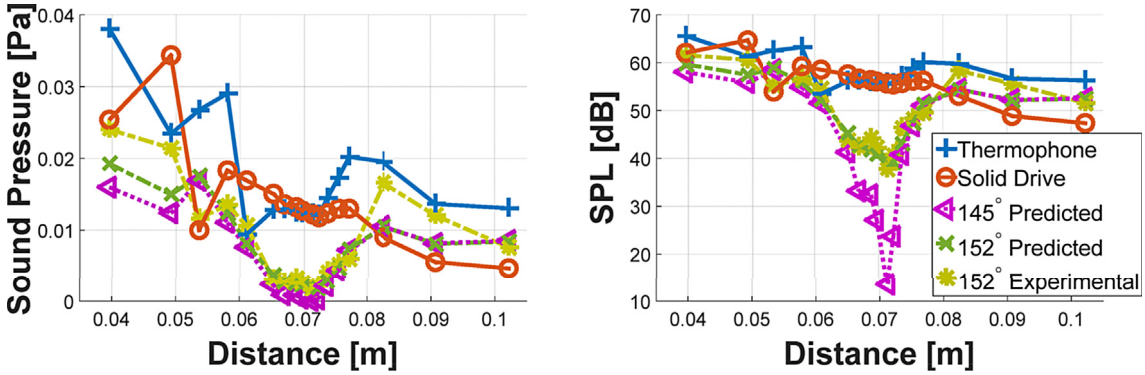

Fig. 13. Sound pressure (left) and SPL (right) along the central axis as a function of microphone distance at a constant frequency of 8 kHz and constant relative phase (in the far field).

acoustic source, while the thermophone transducer is kept unchanged, purple scatter points in Fig. 12. The findings clearly demonstrate the potential of a secondary heat flux source to interfere with a co-axial, co-planar mechanical sound transducer. This is the first ever experimental demonstration of the theorized heat flux driven noise cancelation concept on a source boundary.

Extending the results for other measurement positions is non-trivial due to different size and shapes of the excitation sources. Therefore, it is experimentally investigated by varying the height of the microphone within $4-10.5$ cm, while the frequency is kept constant at 8 kHz (Fig. 13). Initially, the baseline pressure level of each transducer is recorded in isolation at a distance of 7 cm. The two excitation sources are then operated simultaneously, varying the relative phase difference. Maximal noise cancellation is recorded in a relative phase of 152° from the base plate. The data can be compared to the acoustic model, which takes into consideration the interference patterns stemming from different dimensions of the two sources for a relative phase of 145° (purple curve) and 152° (green curve). It can be concluded that relative phase of 145° could result in a more optimal noise cancellation effect, which could not be experimentally demonstrated due to the microphone sensitivity limit.

The relative phase most conducive to noise cancelation is a function of the distance from the excitation sources. This is experimentally validated by maintaining constant individual SPL while varying the phase at each distance. The individual SPLs of the thermophone and the Solid Drive are matched at all heights by adjusting the thermophone power input (blue and red lines in Fig. 14, respectively). At each height, a separate optimum phase for noise cancellation can then be determined experimentally (red line in Fig. 15); and the ensuing locally minimized sound pressure level is charted by green line in Fig. 14. However, using the model predictions towards establishing a theoretical optimum phase (blue line in Fig. 15), an even lower SPL level can be achieved (yellow curve in Fig. 14).

The difference between the experimentally determined phase and theoretical optimal amounts to ~ 10 dB which is almost undetectable by the microphone at these sound pressure levels ($\sim 20-30$ dB). Moreover, the slight deviation is also influenced by contributions from background noise and secondary interferences. Nevertheless, the experimental and theoretically determined optimal phase angles correlate within 10°, Fig. 15.

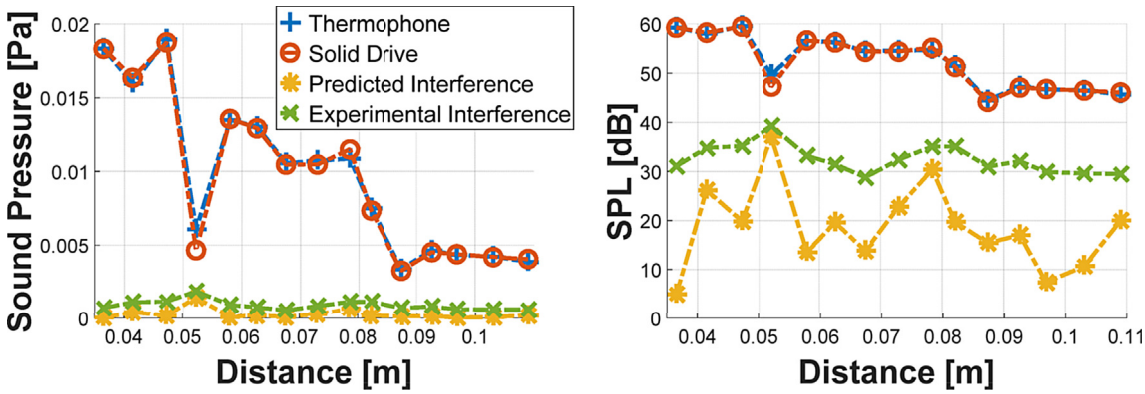

Fig. 14. Noise cancellation at optimal phase and matched power with varied height, at a frequency of 8 kHz in terms of sound pressure (left) and SPL (right) along the central axis (in the far field).

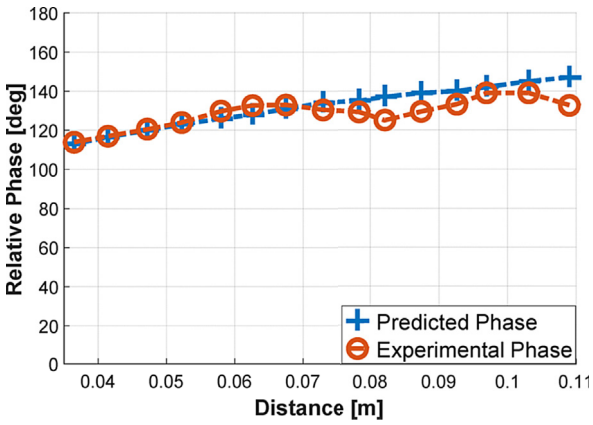

Fig. 15. Variation of optimal noise cancellation phase as a function of microphone distance (in the far field).

8. Summary and conclusions

The scope of this work is focused around noise cancellation concept, which is based upon introduction of a secondary heat flux driven transducer on a vibro-acoustic source boundary. The idea is explored in an experimental setup which consists of a periodically Joule heated substrate deposited over a mechanical speaker. In order to characterize the performance of the two sources, sound propagation theory is coupled with first law of thermodynamics – individually relating heat (thermophone) and work (loudspeaker) with energy. The resulting equations produce a unified acoustic model for a finite area emitter, irrespective of energy source. In the case of thermo-acoustic sound production, the formulation is complemented by thermophone efficiency model. Derived from Fourier heat conduction with internal unsteady generation, diffusive process of energy storage is demonstrated to be the principal driver behind the frequency dependent thermal efficiency variation.

With this concise methodology for modeling the aggregate noise from the vibro- and thermo-acoustic co-planar sources, the sound pressure level is predicted for a broad range of measurement locations. The theoretical findings are validated experimentally, where 68 dB sound pressure generated by a conventional loudspeaker is diminished to 25 dB - well within the background noise. Due to the different size and shapes of the two excitation sources, the noise cancellation occurred at a relative phase angle of 225° for the reference 1.42 cm position. Moreover, the required phase for noise cancellation is adequately predicted by the model (corroborated by experimental data) for all distances from the vibrating boundary.

Despite the advantages offered by thermophone devices, advances in production cost and efficiency must still be made in order to improve their viability for use in common applications. However, if the necessity to be silent holds more value to the user than the additional cost, this technology has tremendous potential. Such consumers would include military, as well as civil applications, which show great interest in advanced noise cancellation methods. Moreover, heating properties can be harnessed beneficially in various systems, such as in suppressing combustion instabilities, while increasing thermal efficiency in a jet engine combustion stage. Demonstrating the feasibility of using heat driven transducers in order to eliminate undesirable acoustic fields directly at the source, the findings highlight the potential of thermophone devices in future active noise cancellation applications.

Funding

This research did not receive any specific grant from funding agencies in the public, commercial, or not-for-profit sectors.

References

[1] C.N. Hansen, Understanding Active Noise Cancellation, CRC Press, 2002.
[2] A. Manela, L. Pogorelyuk, Cloaking via heating: approach to acoustic cloaking of an actuated boundary in a rarefied gas, Phys. Fluids 26 (6) (2014) 062003.
[3] A. Manela, L. Pogorelyuk, Active noise control of a vibrating surface: continuum and non-continuum investigations on vibroacoustic sound reduction by a secondary heat-flux source, J. Sound Vib. 358 (2015) 20–34.
[4] F. Braun, Notiz über thermophonie, Annalen der Physik 301 (6) (1898) 358–360 [Braun, F., Notes about thermophone, Annals of Physics, 1898. 301(6): p. 358-360].
[5] P. Langle, On thermophones, Proc. R. Soc. 91A (1915) 239–241.
[6] H. Hu, Y. Wang, Z. Wang, Wideband flat frequency response of thermo-acoustic emission, J. Phys. Appl. Phys. 45 (34) (2012) 345401.
[7] H. Arnold, I. Crandall, The thermophone as a precision source of sound, Phys. Rev. 10 (1) (1917) 22.
[8] E.C. Wente, The thermophone, Phys. Rev. 19 (4) (1922) 333–345.
[9] H. Shinoda, et al., Thermally induced ultrasonic emission from porous silicon, Nature 400 (6747) (1999) 853–855.
[10] R.R. Boullosa, A.O. Santillan, Ultrasound radiation from simple thermoacoustic transducers, Acta Acustica united Acustica 90 (2) (2004) 277–284.
[11] H. Hu, T. Zhu, J. Xu, Model for thermoacoustic emission from solids, Appl. Phys. Lett. 96 (21) (2010) 214101.

[12] J. Bin, W.S. Oates, K. Taira, Thermoacoustic modeling and uncertainty analysis of two-dimensional conductive membranes, J. Appl. Phys. 117 (6) (2015) 064506.
[13] V. Vesterinen, et al., Fundamental efficiency of nanothermophones: modeling and experiments, Nano Lett. 10 (12) (2010) 5020–5024.
[14] M. Daschewski, et al., Physics of thermo-acoustic sound generation, J. Appl. Phys. 114 (11) (2013) 114903.
[15] L. Xiao, et al., Flexible, stretchable, transparent carbon nanotube thin film loudspeakers, Nano Lett. 8 (12) (2008) 4539–4545.
[16] X. Wang, et al., Fabrication of ultralong and electrically uniform single-walled carbon nanotubes on clean substrates, Nano Lett. 9 (9) (2009) 3137–3141.
[17] A.O. Niskanen, et al., Suspended metal wire array as a thermoacoustic sound source, Appl. Phys. Lett. 95 (16) (2009) 163102.
[18] A.R. Barnard, et al., Feasibility of a high-powered carbon nanotube thin-film loudspeaker, J. Acoust. Soc. Am. 134 (3) (2013) EL276–EL281.
[19] S. Asadzadeh, et al., Thermo acoustic study of carbon nanotubes in near and far field: theory, simulation, and experiment, J. Appl. Phys. 117 (9) (2015) 095101.
[20] A.E. Aliev, Y.N. Gartstein, R.H. Baughman, Increasing the efficiency of thermoacoustic carbon nanotube sound projectors, Nanotechnology 24 (23) (2013) 235501.
[21] T.M. Bouman, A.R. Barnard, M. Asgarisabet, Experimental quantification of the true efficiency of carbon nanotube thin-film thermophones, J. Acoust. Soc. Am. 139 (3) (2016) 1353–1363.
[22] C.W. Lim, L. Tong, Y. Li, Theory of suspended carbon nanotube thinfilm as a thermal-acoustic source, J. Sound Vib. 332 (21) (2013) 5451–5461.
[23] L. Tong, C. Lim, Y. Li, Gas-filled encapsulated thermal-acoustic transducer, J. Vib. Acoust. 135 (5) (2013) 051033.
[24] A.E. Aliev, et al., Underwater sound generation using carbon nanotube projectors, Nano Lett. 10 (7) (2010) 2374–2380.
[25] L. Xiao, et al., High frequency response of carbon nanotube thin film speaker in gases, J. Appl. Phys. 110 (8) (2011) 084311.
[26] M. Daschewski, Thermophony in Real Gases-Theory and Applications, 2016.
[27] H. Tian, et al., Graphene-on-paper sound source devices, ACS Nano 5 (6) (2011) 4878–4885.
[28] J.S. Soares, A. Jorio, Study of carbon nanotube-substrate interaction, J. Nanotechnol. (2012) 2012.
[29] F.A. McDonald, G.C. Wetsel Jr., Generalized theory of the photoacoustic effect, J. Appl. Phys. 49 (4) (1978) 2313–2322.
[30] T.L. Bergman, F.P. Incropera, Fundamentals of Heat and Mass Transfer, John Wiley & Sons, 2011.
[31] C. Multiphysics, Acoustic Module–user's Guide, 2013. Version.
[32] T.A. Brungart, et al., Thermal saturation and its suppression in high-power, compact carbon nanotube thin-film thermophones, in: Proceedings of Meetings on Acoustics 172ASA, ASA, 2016.
[33] H. Hu, D. Wang, Z. Wang, Solution for acoustic field of thermo-acoustic emission from arbitrary source, AIP Adv. 4 (10) (2014) 107114.
[34] M.N. Özışık, Boundary Value Problems of Heat Conduction, Courier Corporation, 1989.